arXiv:2309.10426v1 [cs.RO] 19 Sep 2023

Multi-Object Graph Affordance Network: Enabling Goal-Oriented Planning through Compound Object Affordances

Tuba Girgin Emre Ugur

***Abstract*— Learning object affordances is an effective tool in the field of robot learning. While the data-driven models delve into the exploration of affordances of single or paired objects, there is a notable gap in the investigation of affordances of compound objects that are composed of an arbitrary number of objects with complex shapes. In this study, we propose Multi-Object Graph Affordance Network (MOGAN) that models compound object affordances and predicts the effect of placing new objects on top of the existing compound. Given different tasks, such as building towers of specific heights or properties, we used a search based planning to find the sequence of stack actions with the objects of suitable affordances. We showed that our system was able to correctly model the affordances of very complex compound objects that include stacked spheres and cups, poles, and rings that enclose the poles. We demonstrated the applicability of our system in both simulated and real-world environments, comparing our systems with a baseline model to highlight its advantages.**

I. Introduction

The affordances concept, introduced by J.J. Gibson to refer to the action possibilities provided by the environment [1], has been significantly influential in robotics research in the last decade [2], [3]. Especially developmental aspects of affordances have been widely adopted in robot learning research [4]–[7]. While the previous works explore the affordances of single or paired object interactions, the affordances of compound objects that are composed of an arbitrary number of objects of complex shapes and different sizes have not been sufficiently investigated [8].

Consider an infant trying to build a tower with its toys. Because of the different shapes and sizes of the objects, each one affords different actions. The affordances of the objects may change according to their relations with the other objects in the environment, i.e., while an empty cup is insertable by spheres, an empty cup below a cube can not be insertable anymore. However, if there is a large ring above the cup, it remains insertable. Therefore, the affordance of a tower is formed by the objects in it, but it is not straightforward to model as it also depends on the relative positions of the objects of different affordances. Therefore, we tackle this problem by representing the objects in the compound as a graph, as the graph representation preserves spatial relations between objects, enabling effective reasoning.

In our study, we propose the Multi-Object Graph Affordance Network (MOGAN), which learns features from the graph representations utilizing graph neural networks (GNN) and predicts the effects of an action applied. An action is defined as a pick and place operation of a new object onto the current compound object. The effects are the spatial displacements between the new objects and the objects in the compound structure. Because the objects have complex shapes, sophisticated effects are considered, and a suitable novel effect representation is used. In the end, the learned affordances are represented as the relations of the compound object, the new single object, and the effects.

Tuba Girgin and Emre Ugur are with Deparment of Computer Engineering, Bogazici University, Istanbul, Turkey.

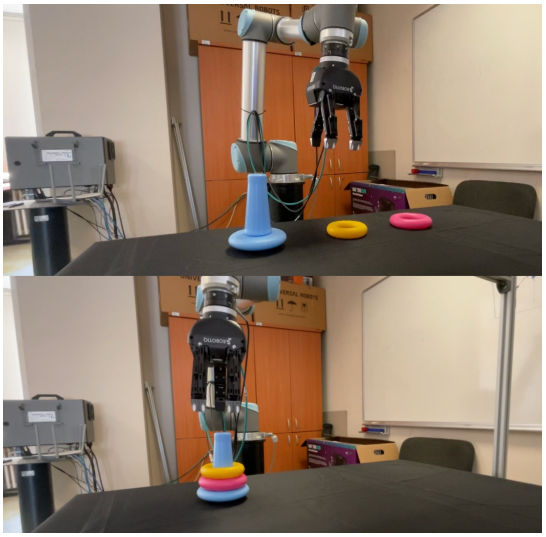

Fig. 1. Execution of the plan generated using our MOGAN model to build the shortest compound object in the real world.

We designed six different tasks using an inventory of single objects, including poles, cups and rings of different sizes, boxes, and spheres. The affordances learned through our model, MOGAN, were utilized to plan a sequence of pick and place actions for constructing a compound object to accomplish a desired task. The results of our model were compared with those of the baseline model that concatenates features of the compound object and the single object instead of a graph structure.

In summary, we propose the MOGAN model that learns affordances given an input graph and an action, and a novel effect encoding to represent the generated sophisticated effects. We showed the applicability of our system, achieving the various tasks in the simulation environment and the real world.

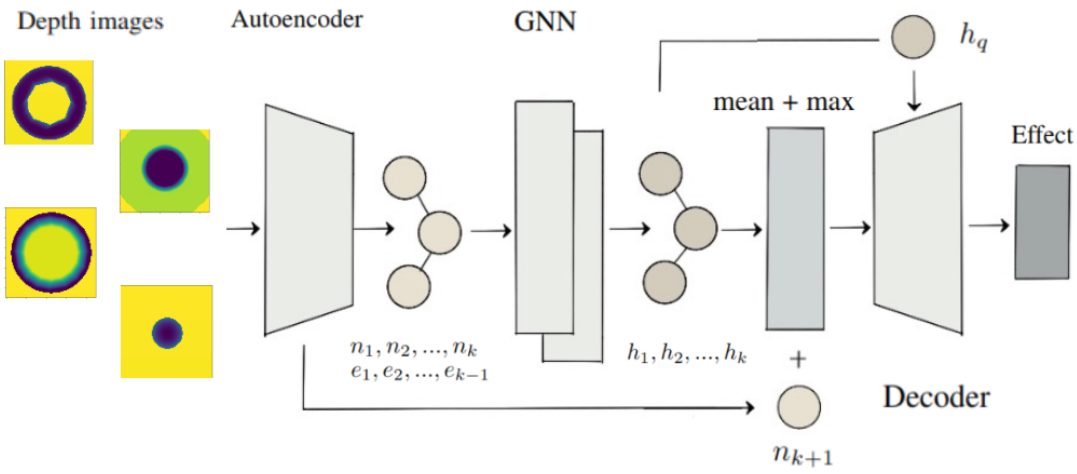

Fig. 2. MOGAN: Multi-Object Graph Affordance Network Architecture. The depth images of single objects are encoded with the autoencoder. It then constructs the graph representation of the compound object. The proposed model, MOGAN, extracts meaningful features from the graph and predicts the resulting effects between a single object and a queried object within the compound object.

II. Related Work

A. Affordances

The study of affordances has attracted significant attention in recent years. [9] detects affordances of objects in images along with their classes, with affordances being labeled at the pixel level. This study focuses on designing a novel network architecture to predict affordances and classes simultaneously, with no emphasis on robotic applications such as robot-environment interactions and planning. Various robotics research benefits affordances to enhance precision in grasping, picking, and placing operations. [10] designs a ROS package enabling the operators to specify grasp poses. [11] learns grasping policies utilizing 3D thermal affordance maps. Learning contact information as affordances, as studied in [12] and [13], is another way to tackle the existing problems. [14] designs a self-supervised affordance learning model that labels gripper open and close points while the robot is controlled through human teleoperation. [15] extends this work, grounding large language models to robotic applications. While these studies supervise their models to learn affordances using contact points and gripper signals, we consider the effects of the manipulator's actions to explore the affordances.

Multiple approaches have studied the exploration of affordances learning effects through interactions [16], [17]. [18] explores affordance categories according to the effects of tool usage. They map the features extracted from the observations and affordance classes discovered by clustering the effects with the k-means algorithm. [19] define affordances as the probability of effects given the object features, tool features, and action. With the formulation of goals as symbols, they achieve probabilistic planning. [20], [21] also performed subsymbolic and symbolic planning, using affordances of only single or paired objects. In our study, we adapt deep neural network architectures to exploit their representation capacity for compound object affordances.

B. Graph Neural Networks

Graph Neural Networks are effective for learning meaningful representations of compound structures and their relations. Consequently, it has gained extensive adoption to reason relations between multi-object systems [22]–[25].

[26] represents multi-object scenes as fully connected graph structures based on partial observations. They design their tasks using logical rules and learn them as the relations between nodes. A search algorithm plans an action sequence to accomplish the desired task. In our study, we learn relations between complex objects through observed effects without defining logical symbols. [27] designs a GNN architecture by learning point-wise affordances from a point cloud dataset. [28] learns actions depicted in images, designing a GNN model with the concept of affordances. They represent humans and objects in the images as nodes of the graph to learn the relations between them. This study focuses on human-object interactions through images, while our study takes advantage of the observations, actions, and effects derived from a dynamic setup.

Overall, in our study, we represent compound objects as graph structures, learn their features utilizing GNNs, and learn the affordances through effect predictions. We plan a sequence of actions (selecting an object to place it on the compound object) with a search algorithm utilizing the learned affordances.

III. Method

Our proposed method models the affordances of compound objects, which are composed of an arbitrary number of objects that are placed on top of each other. Given the compound object and a new object, it learns to predict the effects generated by placing the new object on top of the compound object. In our framework, an affordance, which is denoted as A, is defined as the relation between the compound object (T) that resides on the table, the object (o) that is placed on top of the compound object, and the

effect (E) generated: $A = (T, o, E)$. Given T and o, our system is expected to learn to predict E.

For learning, at each step, the robot randomly selects and picks up an object, places it on top of the current object compound, and observes the effects until either the new object falls down or the object compound collapses. At the start of each exploration cycle, the size of the object compound is initialized as 0. In the rest of this section, we first describe how compound and single objects (T and o) and effects (E) are represented, and the details of the learning algorithm. Finally we describe how the learned affordances can be used to make plans in order to achieve different goals.

A. Single Object Representation

The single objects are represented with autoencoder features obtained from their depth images. The encoder part of the autoencoder receives a 32x32 normalized depth image and consists of 3 linear layers with neuron sizes 256, 256, and 64, respectively. The latent space size 4 was found to be sufficient empirically in order to represent the images of the set of the objects used in this study. The decoder part is the reverse of the encoder. When collecting the learned hidden representations, the maximum and minimum values of the depth images are appended to prevent the information loss caused by the normalization operation. Therefore, the single objects o are represented with a feature vector of size 6.

B. Compound Object Representation

The compound objects are composed of different objects placed on top of each other. In order to represent a compound object, both the features of the single objects inside the compound and the spatial relations between the objects are required to be used. For this, we utilize a graph-based structure. A graph, denoted as G, is defined as a tuple of nodes N and edges E.

$$G = (N, E)$$

$$N = \{n_1, n_2, ..., n_k\}, n_i \in \mathbb{R}^p, 1 \leq i \leq k$$

$$E = \{e_1, e_2, ..., e_{k-1}\}, e_i \in \mathbb{R}^q, 1 \leq i \leq k-1.$$

Each node, n, consists of the object features acquired through the autoencoder. As described before, the feature size p is set as 6. k indicates the number of nodes within the graph, with no specific limits on this count. A directed edge between two nodes is defined if the objects were placed sequentially in the tower in a direction from the top to the bottom object. All nodes form self-connections.

C. Effect Representation

When an object is placed on the compound object, different types of effects, such as insertion in different ways, stacking, or toppling, are observed. Instead of categorizing each effect instance into a pre-defined effect category, we propose a generic continuous effect representation that captures the 3D spatial relations between the placed object and each object in the compound. In other words, the effect represents the spatial outcome of placing the new object on the compound and is encoded as a combination: $E = [E_1, E_2, E_3]$. E_1 describes the height differences between the top and bottom surfaces of each object pairs.

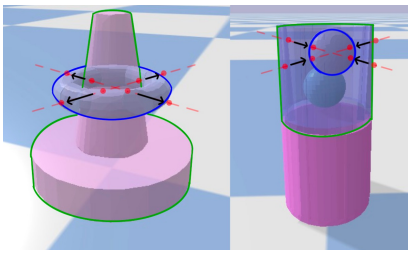

Fig. 3. Visualization of the calculation of lateral spatial displacements: Imaginary rays are projected through the center of the new object. Red points illustrate the intersections with both the compounding object and newly added object. The faces of green object that the rays pass through create positive and negative regions. If the intersection point on the blue object remains in the positive region, the effect's sign becomes positive.

$$E_1 = \{E_1^1, E_1^2, .., E_1^k\}, E_1^i \in \mathbb{R}^2, 1 \leq i \leq k$$

$$E_1^i = \{s(|z_i^+ - z_{k+1}^+|), s(|z_i^- - z_{k+1}^-|)\}$$

E_1^i correpsponds to the effect between the new object and the i^{th} object in the object compound. z^+ and z^- describe the maximum and minimum height values of an object. s is a sign function that assigns signs to the effect values. The faces of the i^{th} object are considered as planes that divide the Cartesian space into positive and negative regions. If the concerned face of the new object remains on the positive side, the sign of the effect becomes positive. Otherwise, it becomes negative.

E_2 encodes the lateral spatial differences between objects. The differences are calculated by sending imaginary rays through the new object, as shown in Fig. 3. If the ray does not intersect with the interested object (outlined with green color), the relevant effect becomes 0. The signs of the differences are calculated with the sign function s considering the faces that the imaginary rays cut.

$$E_2 = \{E_2^1, E_2^2, .., E_2^k\}, E_2^i \in \mathbb{R}^4, 1 \leq i \leq k$$

$$E_2^i = \{s(|x_i^+ - x_{k+1}^+|), s(|x_i^- - x_{k+1}^-|),$$
$$s(|y_i^+ - y_{k+1}^+|), s(|y_i^- - y_{k+1}^-|)\}$$

$$E_3 = \begin{cases} 1, & \text{if } pos(o_i) \geq t_1 || ori(o_i) \geq t_2, 1 \leq i \leq k+1 \\ 0, & \text{otherwise} \end{cases}$$

Finally, E_3 encodes whether the newly placed object falls down or the compound object collapses/topples when the new object is placed on top.

D. Multi-Object Graph Affordance Network (MOGAN)

The proposed MOGAN model, shown in Fig. 2, outputs the effect (E) expected to be generated when a new object (o) is placed on the compound object (T). As the compound object was formed by placing the objects one by one on top of each other, the depth images and the corresponding

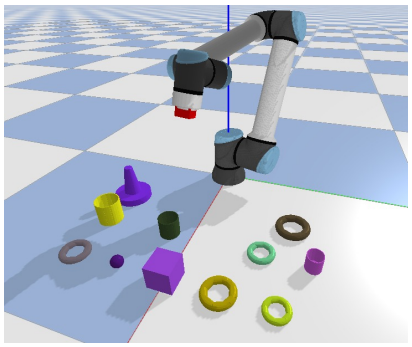

Fig. 4. A PyBullet environment featuring a UR10 robot and various objects, including cubes, poles, spheres, cups, and rings.

Fig. 5. Various objects used in the real-world setup: sticks, rings, cups, cubes, and balls.

autoencoder features $(n_1, n_2, ..n_k)$ were already collected and available for processing. The autoencoder features of the new object to be placed on the compound object are also processed and is represented by n_{k+1} in the figure. MOGAN processes the features of the objects in the compound object and the features of the new object and produces the effect of the placement action.

MOGAN consists of two components: an encoder and a decoder of a graph neural network (GNN). In order to build the layers of the encoder, GCNConv module from the PyTorch Geometric library is used. The encoder generates a latent representation for the input graph. The mean and maximum values of these latent representations are calculated and concatenated to the feature vector of the object to be placed on the compound object. The decoder with linear layers takes these concatenated values along with the hidden representation of the queried node to predict the effects between the node and the new object placed on the top of the tower. The network includes two GCNConv layers and three linear layers, totaling five layers. The parameter size for the network is 46.786. Leaky ReLU is utilized as the activation function. Mean Squared Error (MSE) loss and a custom sign loss are utilized as the loss functions. The sign loss, which is used for E_1 and E_2, penalizes predictions that do not align with the correct signs compared to the ground truth data.

E. Planning and Tasks

We aim to provide a variety of tasks to demonstrate the prediction capacity of the MOGAN for planning to achieve different goals. The goals include obtaining object compounds of specified heights, structures, and sub-structures. A tree search algorithm is realized to discover the optimal plan to achieve a specific goal. At each iterative step, the graph representation of the existing object compound is generated, and the object that will be placed on the tower is encoded. Three MOGAN network predicts the effects E based on the graph representation of the compound and the feature vector of the new object. If predicted E_3 indicates a fall/collapse, the current branch of the search operation is terminated.

In detail, six different tasks can be specified. The first two tasks correspond to building the tallest and shortest compounds/towers. In order to predict the height of the object compounds, the E_1 effect predictions are summed up. The third and fourth tasks correspond to obtaining structures where the placed objects are required to enclose the top part of the object compound and become invisible in the compound (inserted inside). The accumulated E_2 predictions are used for this purpose. The fifth task corresponds to building a tower of a specific height. Finally, the sixth task enables the selection of two objects from the set of objects that will be used in the object compound and puts constraints on their relative placements, such as maximizing or minimizing their relative distances.

F. Experimental Setup

A manipulator robot and a set of objects with different shapes and sizes are used in the simulation and real world experiments. The Pybullet environment is used for simulating actions and interactions. A 7-DOF UR10 manipulator with a Robotiq 3-Finger Adaptive Robot Gripper is used in the real world. A custom gripper is attached to the wrist of the UR10 manipulator in the simulator in order to speed up the pick and place action executions. The objects that are commonly used in the simulator and the real world correspond to sticks, rings, cups, balls, and cubes as shown in Fig. 5 and Fig. 4. A subset of the inventory is spawned in a rectangular area at random positions. The positions of the objects can be acquired by a segmentation algorithm using the depth image of the scene. A Realsense depth camera is attached to the top of the table to obtain the depth images of the real objects. The depth images of the simulated scene are taken with a virtual depth camera. The depth image of the scene is segmented to acquire the depth images of the objects individually. In order to segment the depth image, the lowest values are grouped according to the pixel positions. The image is cropped according to the center pixel positions for each group. The positions of the objects are calculated using the center pixel positions and values and used during pick and place action executions.

IV. Experiments and Results

A. Baseline Model

A baseline model is trained to examine the advantage of the graph neural networks. The features of the nodes are concatenated in a single tensor instead of representing them as a graph. The size of the tensor is the multiplication of the feature size and the maximum object number in a tower. The

TABLE I

COMPARISON OF PLAN SUCCESS RATES IN THE SIMULATION ENVIRONMENT WITH THE BASELINE (B)

Size	**Task 1: Tallest**		**Task 2: Shortest**		**Task 3: Occluded**		**Task 4: Occluding**		**Task 5: Specific Height**		**Task 6: Condition**	
	MOGAN	B	MOGAN	B	MOGAN	B	MOGAN	B	MOGAN	B	MOGAN	B
2	100	80	100	80	100	8 0	100	80	100	90	100	100
3	100	60	100	80	100	90	100	70	90	60	100	60
4	90	50	90	80	80	80	90	60	90	60	90	60
5	80	10	90	60	90	40	80	60	80	50	90	60

TABLE II

PREDICTION ERRORS FOR THE UNSEEN SIMULATION DATA

Tower Size	Test Errors		
	Effect 1 (dm)	Effect 2 (dm)	Effect 3
1	0.000	0.000	0.010
2	0.008	0.000	0.099
3	0.022	0.004	0.149
4	0.043	0.003	0.177
5	0.063	0.002	0.177
6	0.085	0.002	0.184
7	0.093	0.001	0.240
8	0.109	0.001	0.145
9	0.126	0.000	0.185
10	0.141	0.000	0.231
11	0.134	0.000	0.306
12	0.123	0.000	0.322
13	0.092	0.000	0.330
14	0.108	0.000	0.252

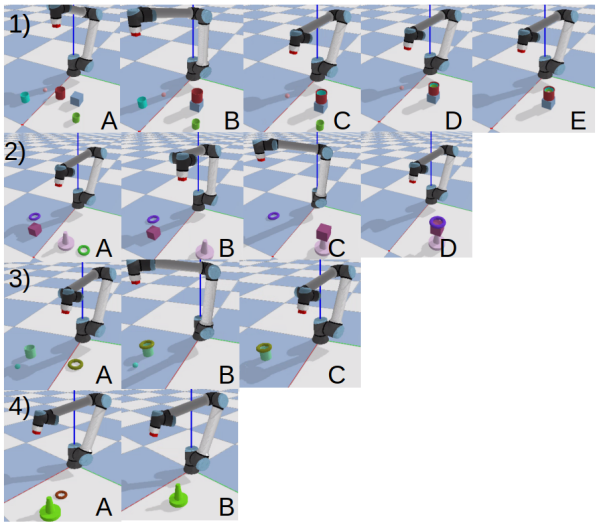

Fig. 6. A number of sample plan executions in the simulator. The task is (1) to build the shortest compound object using a cube, three different sized cups, and a sphere, (2) to build a compound object giving a constrain as maximizing the relational height differences of the rings, (3) to maximize the invisibility of objects, (4) to build the tallest compound object given a ring and pole.

maximum object number extracted from the dataset is 14 in our case. The remaining part of the input tensor remains 0 for the smaller-sized object compounds. Two linear layers are utilized to encode the concatenated features. The effect is the concatenation of all effects for each node in a tower. The parameter size for the baseline model is 50178, which is close to the parameter size of our proposed model. Training and test results are compared with the MOGAN model in the Experiments and Results Section.

B. Results

1) Effect Prediction Accuracy: In this section, we analyze the prediction error of our model for the unseen test data and provide the results in Table II. The errors are grouped according to the compound object sizes to analyze the relation between compound object sizes and prediction errors. Effect 1 is the predicted height differences between two objects, as explained in the Method Section. The inventory contains objects with maximum, minimum, and mean height values of 17 cm, 1.5 cm, and 6.5 cm, respectively. The errors in Effect 1 predictions result in deviations of less than 1 cm in predicted height differences when the compound object size is 8 or less. If the object size exceeds 8, we observe a maximum error of 1.41 cm. Although these prediction errors do not significantly impact the majority of predictions due to the presence of considerably larger objects, they can lead to failures when predicting effects between smaller objects, such as small rings. The error for Effect 2 does not increase along with the compound object size. We can confidently state that our model is capable of predicting x and y displacements of objects without being affected by the number of objects. The ground truth value of Effect 3 is 1 when the tower collides, 0 otherwise. When we inspect the prediction errors for Effect 3, we see that it increases as the number of objects increases. However, the errors in Effect have minimal impact on the overall results due to the margin between ground truth values.

C. Simulation Experiments & comparison with Baseline

We evaluate the generated plans for six different tasks, we sample 10 different configurations for each compound object size, ranging from 2 to 5 in the simulator. For the fifth task, which is to build a compound object with a desired height, we calculated possible height values for the sampled configuration, selected one as the goal, and compared it to the resulting height. For the last task, we randomly selected two objects from the sampled set of objects to maximize or minimize their distances. Please see the generated and executed plans for a number of sample tasks in Fig 6. Out of 300 planning tasks, our system was able to generate 283 successful plans, as shown in Table I. The success rate was observed to slightly drop when the number of objects increases. This was an expected result, as the number of objects in the compound increase, predicting the affordance of the compound object and how it is affected from placing

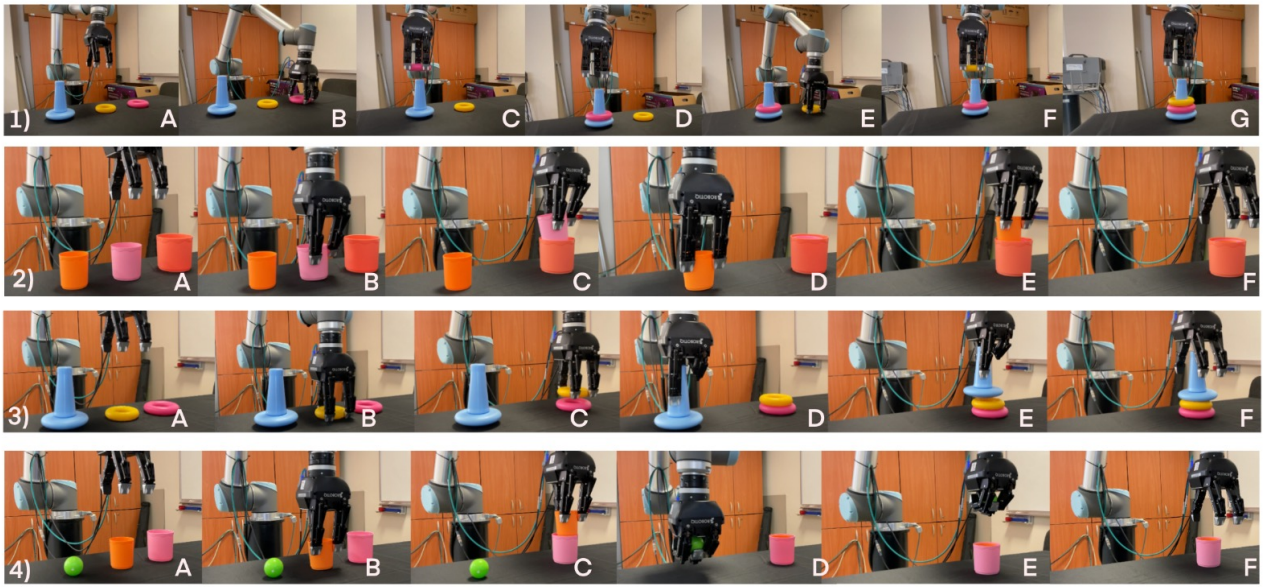

Fig. 7. A number of snapshots from real-world planning experiments. In the first, second, and fourth images, the objective is to construct the shortest compound objects. In the third image, the goal is to create the tallest compound object. The system observes the scene, predicts the effects of each potential plan using MOGAN, and executes the optimal one.

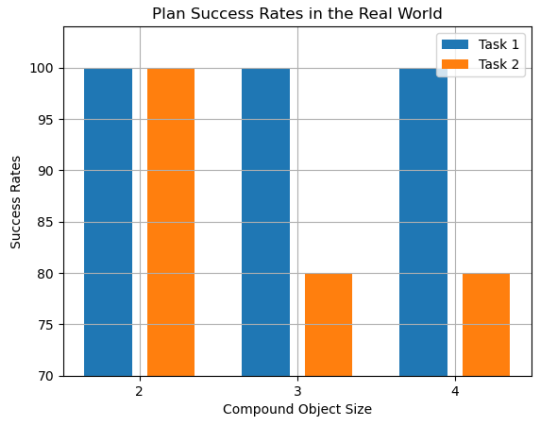

Fig. 8. Plan success rates in the real world. The goals are to build the shortest and tallest compound objects. 5 trials were conducted for each set of different sizes.

another object on top becomes more difficult. Additionally, as the number of objects increases, the number of predictions done during the planning increases exponentially. One erroneous prediction among all the correct predictions may cause a failure in planning. It is important to note that our MOGAN model significantly outperformed the base model in planning, as shown in Table I, showing the effectiveness of using graph structures where the features of the objects in the compound are embedded in the nodes of the GNN for modeling multi-object affordances and for the multi-object planning problems.

D. Real-world Experiments

In the real-world setup, we test our system's planning capacity with the first two tasks: building the shortest and the tallest compound objects. We sampled 5 different sets of objects for the compound object sizes 2, 3, and 4. A number of plan execution snapshots from sampled tasks are provided in Fig.7. Out of the 30 real-world planning tasks, 28 of the generated plans were found to be successful, as shown in Figure 8. The system is able to build desired compound objects 1) using the depth images from Realsense, 2) predicting effects with the MOGAN model, 3) planning an optimal path with the tree search algorithm, and 4) executing it with the UR10 manipulator. The success rate slightly decreases as the object number in the inventory increases. Along with the reasons explained, another reason for the failure is the unpredictability of the real-world systems. Because the objects we use are soft and deformable, unexpected results may arise during the open and close operations of the gripper. i.e., when the robot holds the pole, it grips it too tightly. As a result, when the gripper opens, the pole gets stuck between the fingers and does not fall.

V. Conclusion

In this research, we proposed a novel Multi-Object Graph Affordance Network, MOGAN, which models affordances of compound objects for manipulation and planning. We showed that our system was able to correctly predict the affordances of complex compound objects that include spheres, cups, poles, and several rings that enclose the poles. This prediction capability was effectively used to build different structures via planning structures of highly complex affordances. In the future, we plan to diversify the object inventory and action repertoire and investigate symbolic planning capabilities in this complex affordance setting.

REFERENCES

[1] J. J. Gibson, "The theory of affordances," *Hilldale, USA*, vol. 1, no. 2, pp. 67–82, 1977.

[2] E. Rome, L. Paletta, E. Şahin, G. Dorffner, J. Hertzberg, R. Breithaupt, G. Fritz, J. Irran, F. Kintzler, C. Lörken *et al.*, "The macs project: an approach to affordance-inspired robot control," in *Towards Affordance-Based Robot Control: International Seminar, Dagstuhl Castle, Germany, June 5-9, 2006. Revised Papers*. Springer, 2008, pp. 173–210.

[3] L. Jamone, E. Ugur, A. Cangelosi, L. Fadiga, A. Bernardino, J. Piater, and J. Santos-Victor, "Affordances in psychology, neuroscience, and robotics: A survey," *IEEE Transactions on Cognitive and Developmental Systems*, vol. 10, no. 1, pp. 4–25, 2016.

[4] E. Şahin, M. Cakmak, M. R. Doğar, E. Uğur, and G. Üçoluk, "To afford or not to afford: A new formalization of affordances toward affordance-based robot control," *Adaptive Behavior*, vol. 15, no. 4, pp. 447–472, 2007.

[5] E. Ugur, E. Oztop, and E. Sahin, "Goal emulation and planning in perceptual space using learned affordances," *Robotics and Autonomous Systems*, vol. 59, no. 7-8, pp. 580–595, 2011.

[6] E. Ugur, Y. Nagai, E. Sahin, and E. Oztop, "Staged development of robot skills: Behavior formation, affordance learning and imitation with motionese," *IEEE Transactions on Autonomous Mental Development*, vol. 7, no. 2, pp. 119–139, 2015.

[7] E. Ugur and J. Piater, "Emergent structuring of interdependent affordance learning tasks," in *4th International Conference on Development and Learning and on Epigenetic Robotics*. IEEE, 2014, pp. 489–494.

[8] P. Zech, S. Haller, S. R. Lakani, B. Ridge, E. Ugur, and J. Piater, "Computational models of affordance in robotics: a taxonomy and systematic classification," *Adaptive Behavior*, vol. 25, no. 5, pp. 235–271, 2017.

[9] T.-T. Do, A. Nguyen, and I. Reid, "Affordancenet: An end-to-end deep learning approach for object affordance detection," in *2018 IEEE international conference on robotics and automation (ICRA)*. IEEE, 2018, pp. 5882–5889.

[10] S. Hart, P. Dinh, and K. Hambuchen, "The affordance template ros package for robot task programming," in *2015 IEEE international conference on robotics and automation (ICRA)*. IEEE, 2015, pp. 6227–6234.

[11] P. Mandikal and K. Grauman, "Learning dexterous grasping with object-centric visual affordances," in *2021 IEEE international conference on robotics and automation (ICRA)*. IEEE, 2021, pp. 6169–6176.

[12] G. Schiavi, P. Wulkop, G. Rizzi, L. Ott, R. Siegwart, and J. J. Chung, "Learning agent-aware affordances for closed-loop interaction with articulated objects," in *2023 IEEE International Conference on Robotics and Automation (ICRA)*. IEEE, 2023, pp. 5916–5922.

[13] Y. Geng, B. An, H. Geng, Y. Chen, Y. Yang, and H. Dong, "Rlafford: End-to-end affordance learning for robotic manipulation," in *2023 IEEE International Conference on Robotics and Automation (ICRA)*. IEEE, 2023, pp. 5880–5886.

[14] J. Borja-Diaz, O. Mees, G. Kalweit, L. Hermann, J. Boedecker, and W. Burgard, "Affordance learning from play for sample-efficient policy learning," in *2022 International Conference on Robotics and Automation (ICRA)*. IEEE, 2022, pp. 6372–6378.

[15] O. Mees, J. Borja-Diaz, and W. Burgard, "Grounding language with visual affordances over unstructured data," in *2023 IEEE International Conference on Robotics and Automation (ICRA)*. IEEE, 2023, pp. 11 576–11 582.

[16] B. Moldovan, P. Moreno, M. Van Otterlo, J. Santos-Victor, and L. De Raedt, "Learning relational affordance models for robots in multi-object manipulation tasks," in *2012 ieee international conference on robotics and automation*. IEEE, 2012, pp. 4373–4378.

[17] B. Moldovan and L. De Raedt, "Occluded object search by relational affordances," in *2014 IEEE International Conference on Robotics and Automation (ICRA)*. IEEE, 2014, pp. 169–174.

[18] T. Mar, V. Tikhanoff, G. Metta, and L. Natale, "Self-supervised learning of grasp dependent tool affordances on the icub humanoid robot," in *2015 IEEE International Conference on Robotics and Automation (ICRA)*. IEEE, 2015, pp. 3200–3206.

[19] A. Antunes, L. Jamone, G. Saponaro, A. Bernardino, and R. Ventura, "From human instructions to robot actions: Formulation of goals, affordances and probabilistic planning," in *2016 IEEE International Conference on Robotics and Automation (ICRA)*. IEEE, 2016, pp. 5449–5454.

[20] E. Ugur, E. Şahin, and E. Oztop, "Unsupervised learning of object affordances for planning in a mobile manipulation platform," in *2011 IEEE International Conference on Robotics and Automation*. IEEE, 2011, pp. 4312–4317.

[21] A. Ahmetoglu, M. Y. Seker, J. Piater, E. Oztop, and E. Ugur, "Deepsym: Deep symbol generation and rule learning for planning from unsupervised robot interaction," *Journal of Artificial Intelligence Research*, vol. 75, pp. 709–745, 2022.

[22] P. Battaglia, R. Pascanu, M. Lai, D. J. Rezende *et al.*, "Interaction networks for learning about objects, relations and physics," in *Advances in neural information processing systems*, 2016, pp. 4502–4510.

[23] M. B. Chang, T. Ullman, A. Torralba, and J. B. Tenenbaum, "A compositional object-based approach to learning physical dynamics," *arXiv preprint arXiv:1612.00341*, 2016.

[24] Y. Li, J. Wu, J.-Y. Zhu, J. B. Tenenbaum, A. Torralba, and R. Tedrake, "Propagation networks for model-based control under partial observation," in *International Conference on Robotics and Automation*, 2019, pp. 1205–1211.

[25] A. E. Tekden, A. Erdem, E. Erdem, T. Asfour, and E. Ugur, "Object and relation centric representations for push effect prediction," *arXiv preprint arXiv:2102.02100*, 2021.

[26] Y. Huang, A. Conkey, and T. Hermans, "Planning for multi-object manipulation with graph neural network relational classifiers," in *2023 IEEE International Conference on Robotics and Automation (ICRA)*. IEEE, 2023, pp. 1822–1829.

[27] A. Iriondo, E. Lazkano, and A. Ansuategi, "Affordance-based grasping point detection using graph convolutional networks for industrial bin-picking applications," *Sensors*, vol. 21, no. 3, p. 816, 2021.

[28] H. Tan, L. W. 0003, Q. Zhang, Z. Gao, N. Zheng, and G. Hua, "Object affordances graph network for action recognition." in *BMVC*, 2019, p. 145.